

High-yield synthesis and optical properties of g-C₃N₄

Yuan, Yanwen; Zhang, Lulu; Xing, Jun; Utama, M. Iqbal Bakti; Lu, Xin; Du, Kezhao; Li, Yongmei; Hu, Xiao; Wang, Shijie; Genç, Aziz; Dunin-Borkowski, Rafal; Arbiol, Jordi; Xiong, Qihua

2015

Yuan, Y., Zhang, L., Xing, J., Utama, M. I. B., Lu, X., Du, K., et al. (2015). High-yield synthesis and optical properties of g-C₃N₄. *Nanoscale*, 7(29), 12343-12350.

<https://hdl.handle.net/10356/82867>

<https://doi.org/10.1039/C5NR02905H>

© 2015 The Royal Society of Chemistry. This is the author created version of a work that has been peer reviewed and accepted for publication by Nanoscale, The Royal Society of Chemistry. It incorporates referee's comments but changes resulting from the publishing process, such as copyediting, structural formatting, may not be reflected in this document. The published version is available at: [<http://dx.doi.org/10.1039/C5NR02905H>].

Downloaded on 13 Mar 2024 15:07:00 SGT

High-yield Synthesis and Optical Properties of g-C₃N₄

Yanwen Yuan,^a Lulu Zhang,^a Jun Xing,^a M. Iqbal Bakti Utama,^a Xin Lu,^a Kezhao Du,^a Yongmei Li,^b Xiao Hu,^b Shijie Wang,^c Aziz Genç,^d Rafal Dunin-Borkowski,^e Jordi Arbiol^{df} and Qihua Xiong^{*ag}

Graphitic carbon nitride (g-C₃N₄), a metal-free semiconductor with a band gap of 2.7 eV, has received considerable attention owing to its fascinating photocatalytic performances under visible-light. g-C₃N₄ exhibits high thermal and chemical stability and non-toxicity such that it has been considered as the most promising photocatalyst for environmental improvement and energy conservation. Hence, it has great importance to obtain high-quality g-C₃N₄ and gain a clear understanding of its optical properties. Herein, we report a high-yield synthesis of g-C₃N₄ products via heating of high vacuum-sealed melamine powder in an ampoule at temperatures between 450–650°C. Using transmission electron microscopy (TEM), scanning transmission electron microscopy (STEM), electron energy loss spectroscopy (EELS), thermal gravimetric analysis (TGA), X-ray diffraction (XRD), and X-ray photoelectron spectroscopy (XPS), the chemical composition and crystallization of the as-produced g-C₃N₄ are demonstrated. A systematic optical study of g-C₃N₄ is carried out with several approaches. The optical phonon behavior of g-C₃N₄ is revealed by the infrared and Raman spectroscopy, and the emission property of g-C₃N₄ is investigated using photoluminescence (PL) spectroscopy, while the photocatalytic property is explored by the photodegradation experiment.

Received 00th January 20xx,
Accepted 00th January 20xx

DOI: 10.1039/x0xx00000x

www.rsc.org/

Introduction

Graphitic carbon nitride (g-C₃N₄), one of the carbon nitride allotropes, has a graphene-like layered structure composed of heptazine units and the bridge amino groups. With a bandgap of 2.7 eV, g-C₃N₄ exhibits outstanding photocatalytic performance in various photochemical reactions, such as in photodegradation and photocatalytic water splitting under visible light.^{1–5} Unlike traditional organic semiconductors, g-C₃N₄ has excellent thermal and chemical stability, and it is also pollution-free, earth-abundant, inexpensive and facile to produce.⁶ Therefore, g-C₃N₄ is a very competitive candidate for depollution and solar energy development. The high-quality preparation and optical properties of g-C₃N₄ are thus of sustained interest.⁷

Great efforts are made to obtain high quality g-C₃N₄ in previous literature.^{8–10} High-yield synthesis of nano-sized g-C₃N₄ form bulk g-C₃N₄ has been reported recently as well.¹¹ However, the most commonly used approach for the bulk g-C₃N₄ preparation is still by heating reagent in air, such as cyanamide, dicyandiamide, or melamine.^{12, 13} This one-step method is simple and easy to control; however, it suffers from a very low yield (~6%) because the polymerization temperature of g-C₃N₄ is higher than the sublimation point of the reagent, causing the reagent loss before reaction occurs.¹⁴ On the other hand, air contains many gas components such as oxygen and nitrogen, so there may be oxidation or other unexpected reaction during the heating process. To solve the problem on purity and yield, we choose to synthesize g-C₃N₄ in a vacuum-sealed environment.^{15, 16} In this paper, all reagents are sealed inside an evacuated ampoule at the pressure of 3–10 mbar and then heated to the targeted reaction temperature. Since the reagent is not able to escape from the sealed ampoule, a high yield production of g-C₃N₄ (~61%) is achieved. Additionally, there is negligible contamination or oxidation of the g-C₃N₄ products since the heating process is in vacuum. With TEM, STEM-EELS, TGA, XRD and XPS, the composition and structure of the as-produced g-C₃N₄ are characterized to demonstrate the good quality g-C₃N₄ produced via our synthesis approach.

Optimizing the optical properties of g-C₃N₄ is also of great importance to achieve better performance in photocatalytic reactions. As revealed by the state-of-the-art optical studies of g-C₃N₄, different heating temperature of carbon nitride may lead to the change in chemical structure of the sample.^{17, 18} A blue- or red-shift of the photoluminescence may also occur.¹

^a Division of Physics and Applied Physics, School of Physical and Mathematical Sciences, Nanyang Technological University, 637371, Singapore.

^b School of Materials Science and Engineering, Nanyang Technological University, 639798, Singapore.

^c Institute of Materials Research & Engineering, Agency for Science, Technologies and Research, 3 Research Link, 117602, Singapore.

^d Institut de Ciència de Materials de Barcelona, ICMA-B-CSIC, Campus de la UAB, 08193 Bellaterra, Spain.

^e Ernst Ruska-Centre for Microscopy and Spectroscopy with Electrons and Peter Grünberg Institute, Forschungszentrum Jülich GmbH, D-52425 Jülich, Germany

^f Institució Catalana de Recerca i Estudis Avançats, ICREA, Passeig Lluís Companys, 23, 08010 Barcelona, Spain

^g NOVITAS, Nanoelectronics Centre of Excellence, School of Electrical and Electronic Engineering, Nanyang Technological University, 639798, Singapore.

* Email: Qihua@ntu.edu.sg

† Electronic Supplementary Information (ESI) available: (1) STEM-HAADF, STEM-EELS and XRD result of hydrogen-bonded sample. (2) Raman and IR peak positions and their related modes and descriptions of vibration. (3) The Gaussian fitting of PL emission spectra of the g-C₃N₄ sample. (4) PL emission spectra of the g-C₃N₄ products in water. See DOI: 10.1039/x0xx00000x

¹⁹⁻²¹ Following these works, we obtained a series of products from various heating temperatures and carried out the optical characterization including infrared, Raman, and PL spectroscopy to reveal the phonon behavior and the chemical bonds of the g-C₃N₄ products. We also observe a tunable PL emission in the g-C₃N₄ products processed under different temperature and attribute this phenomenon to the extension of the g-C₃N₄ network under increasing temperature. Moreover, photocatalytic decomposition experiment using g-C₃N₄ products is demonstrated, corroborating to the excellent photocatalytic properties of the g-C₃N₄ products.

Experimental Section

Materials synthesis

50 mg of melamine powders were firstly sealed in a quartz ampoule with a diameter of 13 mm and a length of 6-8 cm, after which the ampoule was pumped down to 3-10 mbar. Then, the ampoule is placed in the central region of a quartz tube furnace and heated at a ramp-up rate of 8°C/min to the designated temperatures between 450-650°C. The temperature is then held constant for 2 hours. The ampoule was taken out after cooling to room temperature and opened by a glass cutter. The powders inside the ampoule were collected into a 2 ml centrifuge tube and ultrasonicated in deionized water before dispersion. After 10 min centrifugation at the rate of 14650 rpm, the supernatant liquid was discarded. This washing process is repeated for 5 times to remove unreacted melamine. After washing, the powder is dried in an oven at 60°C for 3-5 hours.

Characterization methods

TEM characterizations. The g-C₃N₄ products are dispersed in isopropyl alcohol by ultrasonication and then deposited on a lacey carbon TEM grid. The morphology of the g-C₃N₄ products was observed by transmission electron microscopy (JEOL JEM 1400) with an accelerating voltage of 100 kV.

STEM-EELS characterizations. The STEM-EELS studies of the g-C₃N₄ products were conducted by using a FEI Titan microscope operated at 80 kV under high angle annular dark field (HAADF).

TGA measurements. The weight percent of each composition of the g-C₃N₄ products was determined by TGA (TA Instruments Q500) with a sampling rate of 10°C/min to 800°C in air.

XRD measurements. XRD of the g-C₃N₄ products was performed using Bruker D8 powder X-Ray diffractometry with a Cu K α radiation (1.54056 Å) and sampling rate of 0.8 degree/min.

XPS measurements. To study the chemical bond of the g-C₃N₄ products, XPS measurements were performed in a VG ESCALAB 220i-XL system using a monochromatic Al K α source. The pass energy of the analyzer was set to 10 eV to have a high measurement resolution. The XPS binding energy scale was calibrated with pure Au, Ag, and Cu standard samples by setting the Au 4f_{7/2}, Ag 3d_{5/2}, and Cu 2p_{3/2} peaks at binding energies of 83.98 \pm 0.02 eV, 368.26 \pm 0.02 eV, and 932.67 \pm 0.02 eV, respectively. The binding energy calibrations were made against the C 1s peak to eliminate the charging of the sample during analysis.

Optical properties studies

Fourier transform infrared spectroscopy (FTIR). FTIR (Perkin Elmer Frontier) is used to determine the chemical structure and the optical properties of the products by scanning from 600 cm⁻¹ to 4000 cm⁻¹ for 16 times.

Raman Spectroscopy. Raman scattering spectroscopy measurements were carried out with 785 nm excitation using a micro-Raman spectrometer (Horiba-JY T64000). The laser power is about 0.3 mW and the measurements were conducted under triple mode with 1800 g/mm grating.

Photoluminescence Spectroscopy. The photoluminescence properties were investigated using a micro-Raman spectrometer (Horiba-JY T64000) in the backscattering configuration excited by a He Cd laser (325 nm) with a power intensity of 0.3 mW (single mode, 600 g/mm grating). The liquid nitrogen continuous flow cryostat (Cryo Industry of America, USA) was used to provide a continuous temperature variation from 77 to 300 K.

Photocatalytic degradation experiment

10 mg/l methylene blue and 1g/l g-C₃N₄ products were used in the experiment and mixed with a stirring rate of 800 r/min in dark for 30 min. Then the mixture was moved to the solar simulator for photocatalytic experiment at the same stirring rate. After each designated interval time (5 min, 5 min, 10 min, 10 min, 20 min, 20 min, 40 min), 1 mL sample is collected into a 2 ml centrifuge and centrifuged for 10 min at the rate of 14650 rpm. Then, the UV-VIS absorption spectra of the supernatant liquid were recorded using a Lambda 950 spectrophotometer at room temperature.

Results and Discussion

Preparation and characterization of high-yield g-C₃N₄ products

The formation of a highly crystalline carbon nitride usually follows the self-condensation process of cyanamide, dicyandiamide, or melamine during heating.²²⁻²⁴ In our case, we use melamine as the reagent in a sealed quartz ampoule. The vacuum level inside the ampoule is controlled under 3-10 mbar. With a heating ramp-up rate of 8 centigrade per minute, the ampoules were heated at different temperatures (450, 500, 550, 600, and 650°C) for 2 hours.

As previous literature indicated,²⁵ the melamine will first form melem (an intermediate product during self-condensation of melamine) and then polymerized into g-C₃N₄ network, accompanied by the color change from white (melamine, melem) to yellow (g-C₃N₄). This phenomenon was also observed in our g-C₃N₄ products heated at different temperatures. Figure 1 (a) is the photograph of all the products synthesized at different temperatures. The color of products changes from white (450°C) to pale yellow (500°C), yellow (550°C), brown (600°C), and to dark brown (650°C), which indicate that the composition of the products is changed. For the white color sample, the composition should be melem in majority. The yellower the sample becomes, the more g-C₃N₄ it contains. When the preparation temperature is too high (600-650°C), the sample turns into brown and dark

brown, which may be due to the carbonization of the sample at high temperature.

Figures 1 (b-f) display the TEM images of the carbon nitride products processed under different temperatures. The morphology of products obtained at 450°C and 500°C have a unique rod-like structure, which we suspect to be the hydrogen-bonded framework of melem²⁶. Beside the rods, there are also a few layered flakes with a width of several hundred nanometers in products obtained at 450°C and 500°C. When the preparation temperature is above 550°C, the flakes became the main products and the average size also increased to several micrometers.

To figure out the composition of the rods and flakes, STEM-HAADF and STEM-EELS have been conducted. Figure 1 (g) is the STEM-HAADF image of a flake obtained at 600°C, and Figures 1 (h-i) show the EELS chemical composition maps for C and N, obtained from the flake. Chemical composition maps suggest the fairly homogeneous distribution of C and N throughout the flake. In general, the carbon nitride flake has a relative C composition of $\sim 45 \pm 1$ at.% and a relative N composition of $\sim 55 \pm 1$ at.%, which is almost equal to the nominal compositions of C_3N_4 phase (C: 42.9%, N: 57.1%). Meanwhile, the EELS result from the bulk of the rod (Figure S1) also shows homogeneous distribution of C ($\sim 41 \pm 0.5$ at.%) and N ($\sim 59 \pm 0.5$ at.%). In this latest case, the C/N ratio is smaller than the nominal compositions of C_3N_4 phase, suggesting a composition in good agreement with polymeric melem (C: 37.5-42.9%, N: 62.5-57.1%).

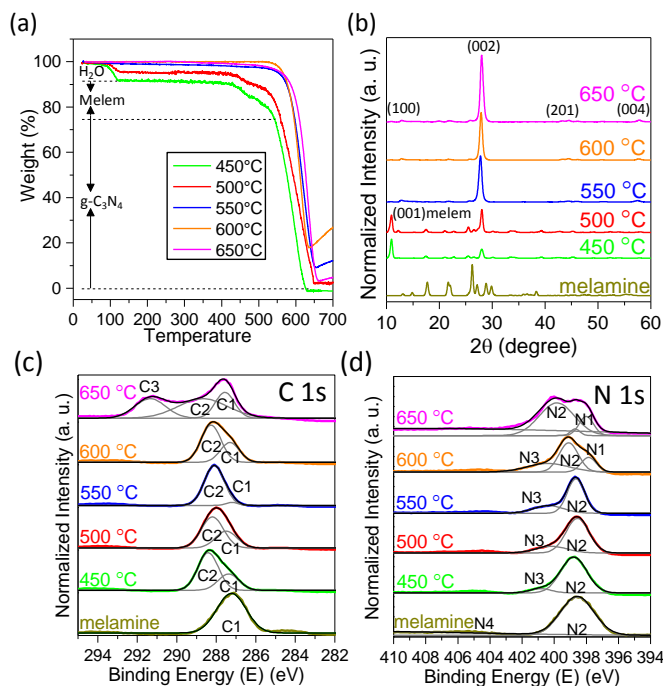


Figure 2 (a) TGA result of the $g-C_3N_4$ products synthesized under different temperatures. The weight loss from room temperature to 100°C is labelled as water and the weight loss from 100°C to 450°C is labelled as melem, meanwhile the weight loss from 450°C to 625°C is labelled as $g-C_3N_4$. (b) Experimental XRD curves of melamine and its heated products. The (100), (002), (201) and (004) directions in $g-C_3N_4$ crystal lattice have been labelled at 13.0°, 27.4°, 44.5° and 57.5° separately, meanwhile the (100) directions in melem crystal lattice have been labelled at 11.0°. (c-d) The normalized XPS spectra of the $g-C_3N_4$ products obtained at different temperatures: (c) C 1s spectrum and (d) N 1s spectrum.

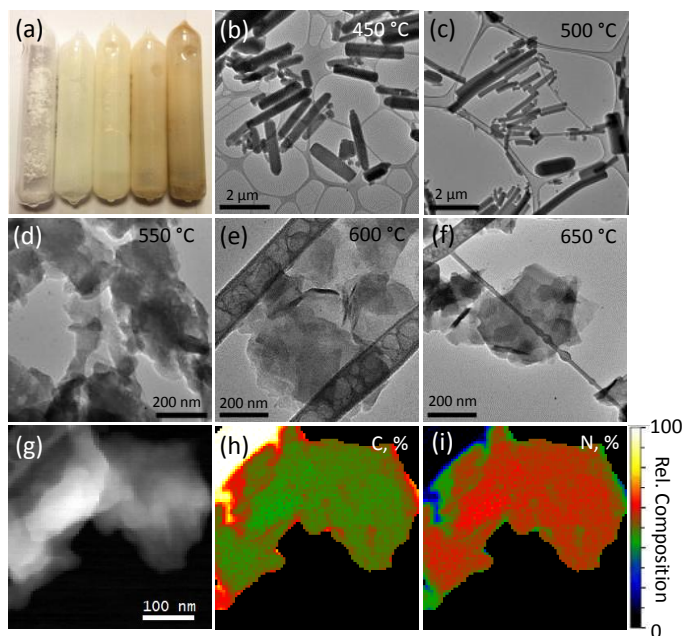


Figure 1 (a) A photograph of the $g-C_3N_4$ products synthesized via the thermal condensation of melamine in vacuum-sealed ampoule under different temperatures (from left to right: 450°C, 500°C, 550°C, 600°C, 650°C). (b-f) TEM images of the products synthesized via the thermal condensation of melamine at 450°C to 650°C. The scale bars of each figure were shown at the bottom. (g) STEM-HAADF micrograph obtained simultaneously during EELS acquisition from the $g-C_3N_4$ flakes within an area of 557 nm x 557 nm. (h-i) Relative compositions of C and N in the elemental mapping. The scale bars of panel (h-i) are same as that of panel (g).

To confirm the content of the $g-C_3N_4$ products, we have conducted further characterizations. Thermal gravimetric analysis (TGA) was performed to find the weight percent of each composition of the heated products. All the samples were heated from room temperature to 700°C at a rate of 10°C/min in air, and the TGA curves are shown in Figure 2 (a). For the samples obtained at 450°C and 500°C, the weight loss at 100°C for bound water (5-10%), 430°C for melem (9-14%) and 550°C for $g-C_3N_4$ (74-77%) were easily identified by their different temperatures of combustion or evaporation. Meanwhile, the samples obtained at 550-650°C shows a high purity of $g-C_3N_4$ level (82-94%), which is in good agreement with the STEM-EELS results. We also observed the weigh increase after 640°C for the samples obtained at 550°C-660°C, and we suspect it might be due to the oxidation of the impurities. Considering the loss from unreacted melamine, melem and impurities, we obtained 30.5 mg $g-C_3N_4$ from 50.0 mg melamine, so the highest yield of $g-C_3N_4$ can achieve up to 61% when the heating temperature is at 550°C. Consider the theoretical yield of 73%, the reaction efficiency from melamine ($C_3N_6H_6$) to $g-C_3N_4$ is almost 84%, this high yield has not been achieved in previous work.

Figure 2 (b) shows the X-Ray Diffraction (XRD) patterns of both melamine and its heated products. As the preparation temperature increases, the melamine index peak has been gradually eliminated. For all the heated products, a strong new peak at 27.4° appeared, representing the typical stacking

structure of g-C₃N₄ layers in (002) direction.²⁷⁻²⁹ And for the samples obtained at 550°C~650°C, there are also few weaker XRD peaks at 13.0°, 44.5° and 57.5°, which represent the (100), (201) and (004) directions in g-C₃N₄ crystal lattice separately.³⁰ In the case of samples obtained at 450°C and 500°C, there is another strong peak at 11.0°, which is the characteristic peak of the hydrogen-bonded framework of melem.²⁶ This hydrogen-bonded framework is formed by the rearrangement of the melem molecules with the appearance of water, and its destruction can be achieved when the sample is heated above 100°C (*i.e.*, the dehydration temperature of crystal water); consequently, the characteristic peak at 11.0° then disappears (SI, Figure S2).

X-ray photoelectron spectroscopy (XPS) was conducted to determine the chemical bonding of the g-C₃N₄ products. In Figures 2 (c) and (d), the high-resolution C 1s and N 1s spectra of both melamine and the g-C₃N₄ products have been collected and then deconvoluted into several Gaussian peaks. In the case of melamine, the C1 peak at 287 eV represents the sp² C atoms in the aromatic ring attached to the -NH₂ group.³¹ After the self-condensation of melamine during annealing, the C1 peak disappeared because of deamination. Instead, the C2 peak originated from sp² C atoms bonded to N inside the aromatic structure, appeared at 288.5 eV.^{32, 33} Remarkably, when the heating temperature is above 600°C, a C3 peak appears at 291 eV. Considering the carbonization of the sample under high temperature, this peak probably comes from the carbon π-π* transition.³⁴ The N 1s spectra also show similar results. For melamine, the strong N2 peak at 399 eV represents the sp² N atoms involved in triazine rings.³⁵ Meanwhile, the N4 peak at 405 eV is contributed by the sp³ N atoms in the amino groups. For the heated products, a new peak (N3 at 401 eV) shows up, which indicates the existence of the bridging sp³ N atoms in N-(C)₃ after reaction.³⁶ When the growth temperature is above 600°C, a weak peak N4 at 398 eV appears. Coupled with the observations of C3 peaks from C 1s spectra, this peak can be assigned to pyridinic N atoms originated from the carbonization of g-C₃N₄.^{37, 38}

Fourier Transform Infrared Spectroscopy (FTIR) and Raman studies of g-C₃N₄ products

To investigate the change in chemical structure during thermal condensation and to gain insight into the optical properties of the g-C₃N₄ products, Fourier transform infrared spectroscopy (FTIR) and Raman spectroscopy were conducted on the samples. Figure 3 (a) shows the FTIR spectra of both melamine and the g-C₃N₄ products. For melamine, the peaks at 3472, 3417, and 3325 cm⁻¹ are attributed to stretching and deformation modes of -NH₂ groups.³⁹ These peaks gradually decreased when the preparation temperature increases, indicating the process of deamination. Meanwhile, the peak at 807 cm⁻¹, which corresponds to the breathing mode of the triazine ring, remains.⁴⁰ There is also a bunch of peaks appearing in the 1100–1650 cm⁻¹ region, which are related to the typical stretching vibration modes of C=N and C–N heterocycles.³² With the increase of the processing temperatures, the position of these peaks also changes. This is

another evidence of the structural change in the thermal condensation reaction.

Using the near-infrared (785 nm) light for excitation, the Raman spectra of the g-C₃N₄ products have been collected. As presented in Figure 3 (b), the fingerprint peaks of melamine at 681 cm⁻¹ (triazine ring breathing mode) and 1566 cm⁻¹ (-NH₂ bending mode) disappeared in the g-C₃N₄ products.^{41, 42} Meanwhile, the signature peaks of g-C₃N₄ at 711 cm⁻¹ (heptazine ring breathing mode) and 1233 cm⁻¹ (stretching vibration modes of C=N and C–N heterocycles) appear.⁹ On the other hand, the baseline of the spectra has a noticeable rise. This may be due to the impurities when the sample is carbonized under high temperature.

Figure 3 (c) zooms in the characteristic peaks of melamine and g-C₃N₄ products obtained under 450–550°C. Clearly, the Raman peaks of g-C₃N₄ emerge gradually along with the increase of preparation temperature. The evolution of Raman spectra exhibits the composition change of g-C₃N₄ products during thermal condensation. And this is also consistent with the characterization result from FTIR. For a better comparison, Raman and IR peak positions observed in this work and their assignment of the vibrational modes has been listed in detail in SI table 1.

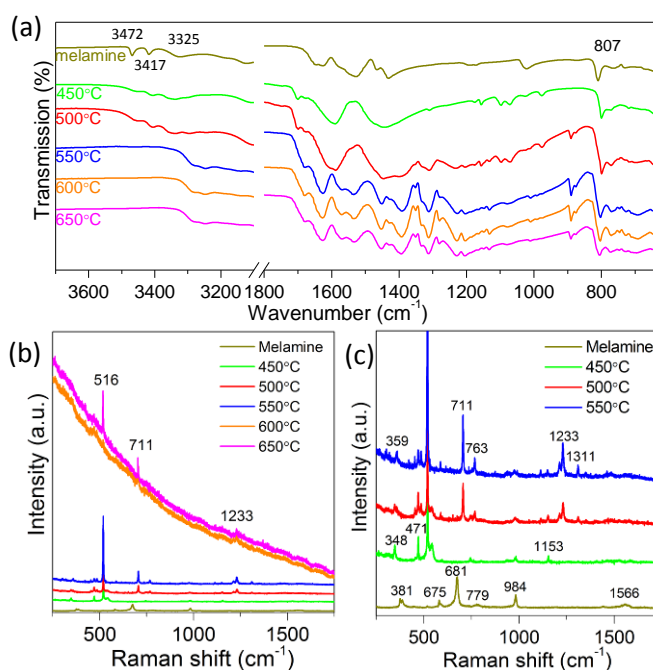


Figure 3. (a) The FTIR spectra of the melamine and the g-C₃N₄ products obtained at different temperatures. (b) The Raman spectra of the g-C₃N₄ products obtained at different temperatures using the near-infrared (NIR 785 nm) light for excitation, in which peak at 516 cm⁻¹ is from silicon substrate, and peaks at 711, 1233 cm⁻¹ are the typical characterization peaks of g-C₃N₄. (c) The zoom-in of Raman spectra of melamine and the g-C₃N₄ products obtained from 450°C to 550°C of (b). The assignment of IR and Raman modes are provided in Table 1 of the Supporting Information.

With all the characterization data above, we can clarify the composition of all the products and figure out the condensation mechanism of $g\text{-C}_3\text{N}_4$. During the heating process inside the ampoule, melamine forms melem by the polymerization of heptazine units, and melem can further be organized into the $g\text{-C}_3\text{N}_4$ network. The efficiency of the reaction is strongly affected by the reaction temperature. When the temperature is below 550°C , the products will contain both melem and $g\text{-C}_3\text{N}_4$ because of incomplete reaction. The percentage of $g\text{-C}_3\text{N}_4$ also increases with the increasing reaction temperature. At 550°C , most of the reagent has transformed into $g\text{-C}_3\text{N}_4$. However, carbonization can also occur when the temperature goes higher. Thus, we conclude that the optimal temperature to produce $g\text{-C}_3\text{N}_4$ with high purity is $\sim 550^\circ\text{C}$.

Emission properties of $g\text{-C}_3\text{N}_4$ products

To understand the emission properties of our $g\text{-C}_3\text{N}_4$ products, we further study their photoluminescence (PL) properties. Figure 4 (a) shows the photographs of the multicolor-emission from melamine and the $g\text{-C}_3\text{N}_4$ products in the same concentration under UV light illumination (365 nm). We can clearly observe the color variation from blue-violet to green. Meanwhile, the intensity of the emission was enhanced at first and quenched later, indicating high purity of $g\text{-C}_3\text{N}_4$ results in high PL intensity.

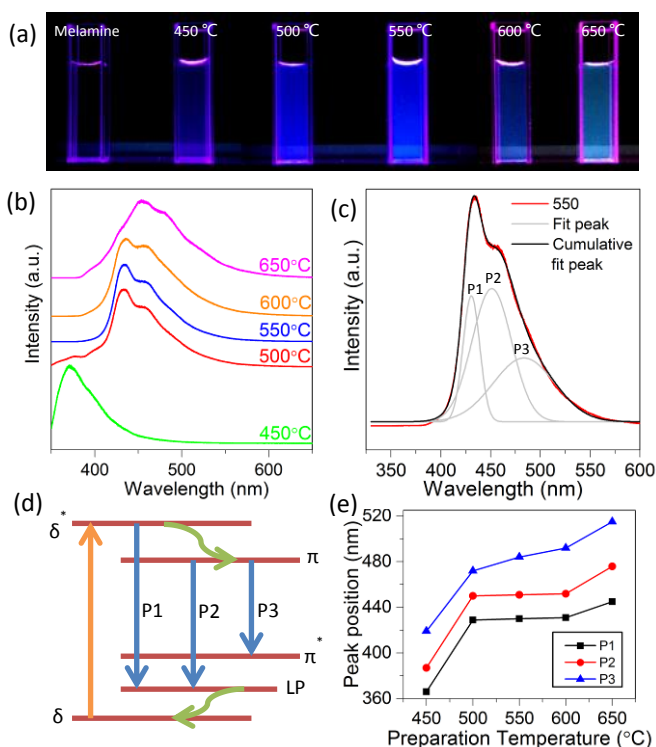


Figure 4. (a) The photographs of the $g\text{-C}_3\text{N}_4$ products in deionized water under UV light (365 nm). (b) The normalized PL emission spectra of the $g\text{-C}_3\text{N}_4$ products using 325 nm laser excitation. (c) The Gaussian fitting of PL emission spectra of 550 °C sample which indicate 3 major PL peaks (P1, P2 and P3). (d) The schematic diagram of the bandgap states of $g\text{-C}_3\text{N}_4$. The orange arrow is the excitation, the blue arrows are the emissions and the green arrows are non-radiative transitions. (e) The peak position of P1, P2 and P3 of the $g\text{-C}_3\text{N}_4$ products obtained under different temperature.

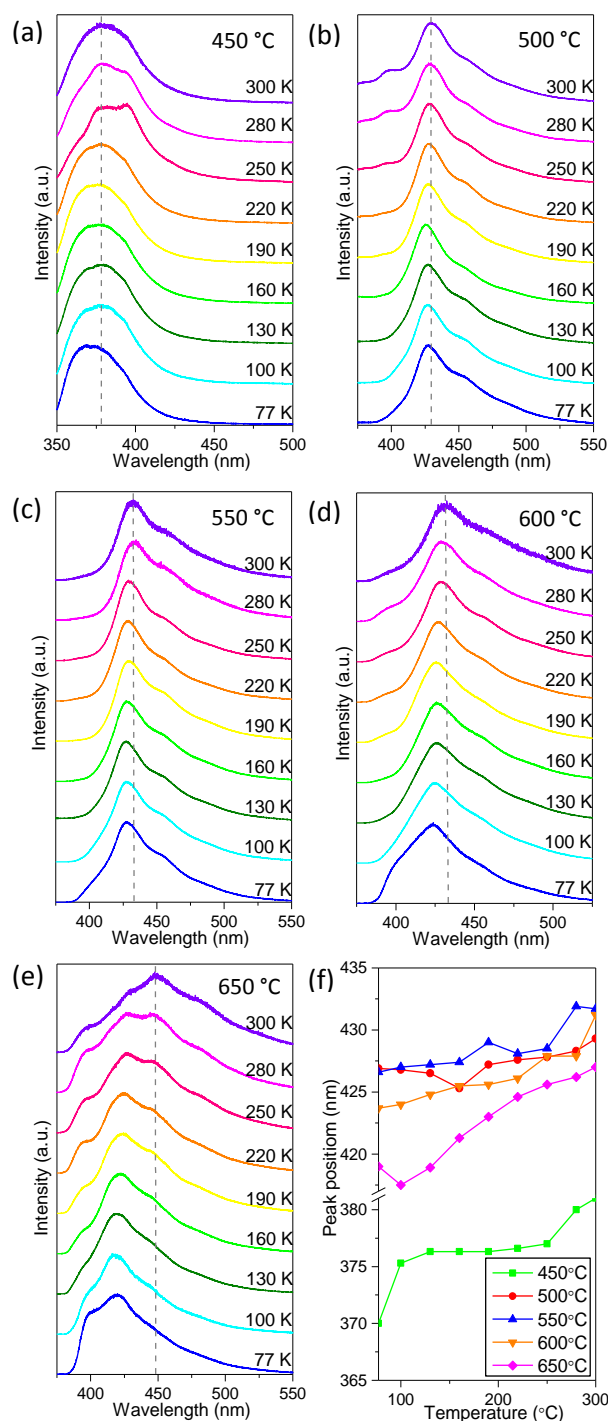


Figure 5. (a-e) The normalized PL emission spectra of the $g\text{-C}_3\text{N}_4$ sample from room temperature (300K) to liquid nitrogen temperature (77K). The sample preparation temperature is labelled on top-right panel. (f) The temperature-dependence of PL peak position change for the $g\text{-C}_3\text{N}_4$ samples obtained under different temperatures.

The steady-state and transient PL emission spectra have been excited by a He-Cd laser (325 nm). The normalized photoluminescence spectra in Figure 4 (b) further prove the red shift of the luminescence center when processing temperature increases from 450°C to 650°C . For melem-rich $g\text{-C}_3\text{N}_4$ sample (450°C), the center of PL spectra is at 369 nm; For $g\text{-C}_3\text{N}_4$ sample (550°C), the center of PL spectra is at 430 nm;

For carbonized g-C₃N₄ sample (650°C), the center of PL spectra is at 455 nm and the peak also become broader because of impurities.

Gaussian fitting of the PL peaks helps us obtain a clear understanding of the nature and origin of excitons in g-C₃N₄ sample. Three major emission centers have been demonstrated in the fitting and decomposition of the emission spectrum of the g-C₃N₄ samples (SI Figure S3). Figure 4 (c) shows the lineshape analysis of g-C₃N₄ sample prepared at 550°C, which include the emission center P1 (429 nm, 2.89 eV), P2 (451 nm, 2.75 eV) and P3 (484 nm, 2.56 eV). According to previous PL study of g-C₃N₄, the bandgap states of g-C₃N₄ consist of sp³ C-N σ band, sp² C-N π band and the lone pair (LP) state of the bridge nitride atom (Figure 4 (d)), and the P1, P2 and P3 origin from the 3 different pathways of transitions: π*-π, σ*-LP and π*-LP respectively.^{20, 43, 44} Figure 4 (e) shows the red shift of P1, P2 and P3 with the preparation temperature increase. This red shift can be explained by the extension of g-C₃N₄ network at higher temperature. When more heptazine is connected by amino group, the π states will hybrid into a broaden state, causing the bandgap narrowing of the sp² C-N clusters.²⁰

Low temperature photoluminescence experiments have been carried out. Figure 5 (a-e) shows the temperature-dependent PL spectra of the g-C₃N₄ sample obtained from 450-650°C. As the temperature decreases, the features of the PL emission spectra are resolved clearer due to the weaker thermal vibration of atoms at low temperature. Meanwhile, the peak position also shows blue shift for about 5-10 nm when the temperature decreases from room temperature to 77 K (Figure 5 (f)). This tunable PL mechanism is mainly attributed to the size reduction of sp² C-N clusters when temperature decreases. Smaller cluster size will result in a larger bandgap and higher probability of the direct transition between the π and π* bands.⁴³ In addition, the LP valence band shifts in the direction of the π band at low temperature,⁴⁵ so the separation between the LP valence and π* bands will increase and cause blue shift in PL emission center. The photoluminescence of carbon nitride in deionized water has also been collected (SI, Figure S4). With water involved, the PL spectra also shows slightly blue shift, which is probably due to the hydrogen-bonding existing in the carbon nitride network, and the LP valence band is affected.

Photocatalytic degradation using g-C₃N₄ products

To investigate the photocatalytic performance of our g-C₃N₄ products, photocatalytic degradation experiments have been performed. Methylene blue was used as the target for degradation and the degradation efficiencies were evaluated by measuring the peak value of the UV-Vis absorption spectra of methylene blue solution. Figure 6 (a) shows irradiation for different durations of 10 mg/L methylene blue after photocatalytic degradation by g-C₃N₄ sample (550°C) under white light from a solar simulator. It can be clearly seen that the absorbance peak of methylene blue gradually decreased, and nearly went down to 0 after 110 mins.

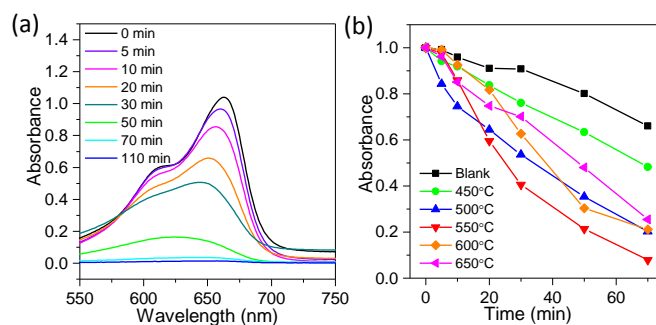


Figure 6. (a) The absorption spectra of 10 mg/L methylene blue after photocatalytic degradation by the g-C₃N₄ products synthesized under 550°C at different time stage. (b) The normalized absorbance of methylene blue with respect to elapsed time after the start of degradation reaction with the g-C₃N₄ products synthesized under different temperature.

The degradation rates of all the g-C₃N₄ products (450-650°C) are summarized in Figure 6 (b). With increasing preparation temperature, the degradation rate of g-C₃N₄ sample first increased, reached the highest point at 550°C, and then finally decreased. Judging from the degradation rate, g-C₃N₄ samples with higher purity have higher photocatalytic activity, indicating that g-C₃N₄ has better oxidability than the by-products of melem or carbonized g-C₃N₄. Moreover, compared with previous literatures, our C₃N₄ sample shows similar photocatalytic performance to the normal air-heated g-C₃N₄ but with a much higher yield.^{4, 46}

Conclusions

In conclusion, we successfully prepared high yield of g-C₃N₄ products using sealed thermal condensation of melamine and investigated the compositional change with the increase of growth temperature. The optical properties and the internal structure of the g-C₃N₄ products have been explored with both FTIR and Raman spectroscopy. Moreover, the PL properties of the g-C₃N₄ products synthesized at different temperatures have been studied. With the increase of synthesis temperature, the carbon nitride products exhibit tunable PL properties. The PL centers vary from blue-violet light region to green light region, which may indicate the optical band gap changes during synthesis. Furthermore, we studied the photocatalytic degradation properties of the g-C₃N₄ products, and concluded that the highest photocatalytic efficiency was obtained at ~550°C growth temperature.

Acknowledgements

Q.X. gratefully thanks Singapore National Research Foundation via a fellowship grant (NRF-RF2009-06), Ministry of Education via a tier2 grant (MOE2012-T2-2-086) and a tier1 grant (2013-T1-002-232). The authors thank Dr. Emrah Yucelen from FEI for his help during the EELS experiments. Some of the research leading to these results has received funding from the European Union Seventh Framework Program under Grant Agreement 312483 - ESTEEM2 (Integrated Infrastructure Initiative – I3). AZ acknowledges German DAAD scholarship program.

Notes and references

1. Y. Wang, X. Wang and M. Antonietti, *Angew. Chem. Int. Ed.*, 2012, **51**, 68-89.
2. K. Maeda, X. Wang, Y. Nishihara, D. Lu, M. Antonietti and K. Domen, *J. Phys. Chem. C*, 2009, **113**, 4940-4947.
3. X. Wang, K. Maeda, A. Thomas, K. Takanabe, G. Xin, J. M. Carlsson, K. Domen and M. Antonietti, *Nat. Mater.*, 2008, **8**, 76-80.
4. S. Yan, Z. Li and Z. Zou, *Langmuir*, 2010, **26**, 3894-3901.
5. J. Liu, Y. Liu, N. Liu, Y. Han, X. Zhang, H. Huang, Y. Lifshitz, S.-T. Lee, J. Zhong and Z. Kang, *Science*, 2015, **347**, 970-974.
6. E. G. Gillan, *Chem. Mater.*, 2000, **12**, 3906-3912.
7. Y. Zheng, J. Liu, J. Liang, M. Jaroniec and S. Z. Qiao, *Energ. Environ. Sci.*, 2012, **5**, 6717-6731.
8. M. L. Cohen, *Mater. Sci. Eng. A*, 1996, **209**, 1-4.
9. S. Tonda, S. Kumar, S. Kandula and V. Shanker, *J. Mater. Chem. A*, 2014, **2**, 6772-6780.
10. H. Yao and W. Ching, *Phys. Rev. B*, 1994, **50**, 11231.
11. Y. Xu, M. Xie, S. Huang, H. Xu, H. Ji, J. Xia, Y. Li and H. Li, *RSC Advances*, 2015, **5**, 26281-26290.
12. S. Yan, Z. Li and Z. Zou, *Langmuir*, 2009, **25**, 10397-10401.
13. S. Wang, C. Li, T. Wang, P. Zhang, A. Li and J. Gong, *J. Mater. Chem. A*, 2014, **2**, 2885-2890.
14. W. Wang, J. C. Yu, D. Xia, P. K. Wong and Y. Li, *Environ. Sci. Technol.*, 2013, **47**, 8724-8732.
15. L. Maya, D. R. Cole and E. W. Hagaman, *J. Am. Ceram. Soc.*, 1991, **74**, 1686-1688.
16. M. Lei, H. Zhao, H. Yang, B. Song and W. Tang, *J. Eur. Ceram. Soc.*, 2008, **28**, 1671-1677.
17. X. Wang, K. Maeda, X. Chen, K. Takanabe, K. Domen, Y. Hou, X. Fu and M. Antonietti, *JACS*, 2009, **131**, 1680-1681.
18. A. B. Jorge, D. J. Martin, M. T. Dhanoo, A. S. Rahman, N. Makwana, J. Tang, A. Sella, F. Corà, S. Firth and J. A. Darr, *J. Phys. Chem. C*, 2013, **117**, 7178-7185.
19. G. Liu, P. Niu, C. Sun, S. C. Smith, Z. Chen, G. Q. Lu and H.-M. Cheng, *JACS*, 2010, **132**, 11642-11648.
20. Y. Zhang, Q. Pan, G. Chai, M. Liang, G. Dong, Q. Zhang and J. Qiu, *Sci. Rep.*, 2013, **3**.
21. H. Zhang and A. Yu, *J. Phys. Chem. C*, 2014, **118**, 11628-11635.
22. S. Muhl and J. M. Mendez, *Diamond Relat. Mater.*, 1999, **8**, 1809-1830.
23. T. Komatsu, *J. Mater. Chem.*, 2001, **11**, 799-801.
24. Y. Zhao, D. Yu, O. Yanagisawa, K. Matsugi and Y. Tian, *Diamond Relat. Mater.*, 2005, **14**, 1700-1704.
25. J. Xu, Y. Li, S. Peng, G. Lu and S. Li, *Phys. Chem. Chem. Phys.*, 2013, **15**, 7657-7665.
26. B. Jürgens, E. Irran, J. Senker, P. Kroll, H. Müller and W. Schnick, *JACS*, 2003, **125**, 10288-10300.
27. Q. Guo, Y. Xie, X. Wang, S. Lv, T. Hou and X. Liu, *Chem. Phys. Lett.*, 2003, **380**, 84-87.
28. A. Thomas, A. Fischer, F. Goettmann, M. Antonietti, J.-O. Müller, R. Schlögl and J. M. Carlsson, *J. Mater. Chem.*, 2008, **18**, 4893-4908.
29. H. Ma, X. Jia, L. Chen, P. Zhu, W. Guo, X. Guo, Y. Wang, S. Li, G. Zou and G. Zhang, *J. Phys.: Cond. Matter*, 2002, **14**, 11269.
30. J. Yang, X. Wu, X. Li, Y. Liu, M. Gao, X. Liu, L. Kong and S. Yang, *Applied Physics A*, 2011, **105**, 161-166.
31. H. Xu, J. Yan, X. She, L. Xu, J. Xia, Y. Xu, Y. Song, L. Huang and H. Li, *Nanoscale*, 2014, **6**, 1406-1415.
32. V. N. Khabashesku, J. L. Zimmerman and J. L. Margrave, *Chem. Mater.*, 2000, **12**, 3264-3270.
33. C. Ronning, H. Feldermann, R. Merk, H. Hofsäss, P. Reinke and J.-U. Thiele, *Phys. Rev. B*, 1998, **58**, 2207.
34. H. Estrade-Szwarckopf, *Carbon*, 2004, **42**, 1713-1721.
35. Y. Li, J. Zhang, Q. Wang, Y. Jin, D. Huang, Q. Cui and G. Zou, *J. Phys. Chem. B*, 2010, **114**, 9429-9434.
36. Y.-A. Li, S. Xu, H.-S. Li and W.-Y. Luo, *J. Mater. Sci. Lett.*, 1998, **17**, 31-35.
37. N. Daems, X. Sheng, I. F. Vankelecom and P. P. Pescarmona, *J. Mater. Chem. A*, 2014, **2**, 4085-4110.
38. Q. Guo, Y. Xie, X. Wang, S. Zhang, T. Hou and S. Lv, *Chem. Commun.*, 2004, **1**, 26-27.
39. M. Jelínek, J. Zemek, M. Trchova, V. Vorlíček, J. Lančok, R. Tomov and M. Šimečková, *Thin Solid Films*, 2000, **366**, 69-76.
40. J. Wei, P. Hing and Z. Mo, *Surf. Interface Anal.*, 1999, **28**, 208-211.
41. P. V. Zinin, L.-C. Ming, S. K. Sharma, V. N. Khabashesku, X. Liu, S. Hong, S. Endo and T. Acosta, *Chem. Phys. Lett.*, 2009, **472**, 69-73.
42. R. Meier, J. Maple, M.-J. Hwang and A. Hagler, *J. Phys. Chem.*, 1995, **99**, 5445-5456.
43. B. Wang, Q. Cheng, L. Wang, K. Zheng and K. Ostrikov, *Carbon*, 2012, **50**, 3561-3571.
44. B. Wang, Q. Cheng, Y. Chen and K. Ostrikov, *J. Appl. Phys.*, 2011, **110**, 054323.
45. G. Fanchini, A. Tagliaferro, N. Conway and C. Godet, *Phys. Rev. B*, 2002, **66**, 195415.
46. L. Song, S. Zhang, X. Wu and Q. Wei, *Chem. Eng. J.*, 2012, **184**, 256-260.